A multilevel optimization approach to route design and flight allocation taking aircraft sequence and separation constraints into account

Ho-Huu, V.; Hartjes, S.; Pérez-Castán, J. A.; Visser, H. G.; Curran, R.

DOI
10.1016/j.trc.2020.102684

Publication date
2020

Document Version
Accepted author manuscript

Published in
Transportation Research Part C: Emerging Technologies

Transportation Research Part C

A multilevel optimization approach to route design and flight allocation taking aircraft sequence and separation constraints into account

--Manuscript Draft--

Manuscript Number:	TRC_2019_1187R3
Article Type:	Research Paper
Keywords:	airport noise; Trajectory Optimization; conflict detection.; aircraft noise; aircraft separation; aircraft allocation
Corresponding Author:	Vinh Ho-Huu Ton Duc Thang University Ho Chi Minh City, Delft Viet Nam
First Author:	Vinh Ho-Huu
Order of Authors:	Vinh Ho-Huu
	Sander Hartjes
	Javier A. Perez-Castan
	Hendrikus Visser
	Richard Curran
Abstract:	This paper presents the development of a multilevel optimization framework for the design and selection of departure routes, and the distribution of aircraft movements among these routes, while taking the sequence and separation requirements for aircraft on runways and along selected routes into account. The main aim of the framework is to minimize aircraft noise impact on communities around an airport, and fuel consumption. The proposed framework features two consecutive steps. In the first step, for each given Standard Instrument Departure (SID), multi-objective trajectory optimization is utilized to generate a comprehensive set of possible alternative routes. The obtained set is subsequently used as input for the optimization problem in the second step. In this step, the selection of routes for each SID and the distribution of aircraft movements among these routes are optimized simultaneously. To ensure the feasibility of optimized solutions for an entire operational day, the sequence and separation requirements for aircraft on runways and along selected routes are included in this second phase. In order to address these issues, three novel techniques are developed and added to a previously developed multilevel optimization framework, viz., a runway assignment model, a conflict detection algorithm, and a rerouting technique. The proposed framework is applied to a realistic case study at Amsterdam Airport Schiphol in the Netherlands, in which 599 departure flights and 13 different SIDs are considered. The optimization results show that the proposed model can offer conflict-free solutions, one of which can lead to a reduction in the number of people annoyed of up to 21%, and a reduction in fuel consumption of 8% relative to the reference case solution.
Suggested Reviewers:	Dan Zachary d.s.zachary@jhu.edu
	Konstantinos VOGIATZIS kvogiatz@civ.uth.gr
	Xavier Prats xavier.prats@upc.edu
	Antonio Filippone A.Filippone@manchester.ac.uk
Response to Reviewers:	

A multilevel optimization approach to route design and flight allocation taking aircraft sequence and separation constraints into account

V. Ho-Huu[a,b*], S. Hartjes[c], J. A. Pérez-Castán[d], H. G. Visser[c], R. Curran[c]

[a] *Division of Computational Mathematics and Engineering, Institute for Computational Science, Ton Duc Thang University, Ho Chi Minh City, Vietnam*
[b] *Faculty of Civil Engineering, Ton Duc Thang University, Ho Chi Minh City, Vietnam*
[c] *Faculty of Aerospace Engineering, Delft University of Technology, P.O. Box 5058, 2600 GB, Delft, The Netherlands*
[d] *Universidad Politécnica de Madrid, ETSIAE, Madrid, 28040, Spain*

E-mails: hohuuvinh@tdtu.edu.vn (V. Ho-Huu)
s.hartjes@tudelft.nl (S. Hartjes)
javier.perez.castan@upm.es (J. A. Pérez-Castán)
h.g.visser@tudelft.nl (H. G. Visser)
r.curran@tudelft.nl (R. Curran)
*Corresponding author: V. Ho-Huu, hohuuvinh@tdtu.edu.vn

Abstract

This paper presents the development of a multilevel optimization framework for the design and selection of departure routes, and the distribution of aircraft movements among these routes, while taking the sequence and separation requirements for aircraft on runways and along selected routes into account. The main aim of the framework is to minimize aircraft noise impact on communities around an airport, and the associated fuel consumption. The proposed framework features two consecutive steps. In the first step, for each given Standard Instrument Departure (SID), multi-objective trajectory optimization is utilized to generate a comprehensive set of possible alternative routes. The obtained set is subsequently used as input for the optimization problem in the second step. In this step, the selection of routes for each SID and the distribution of aircraft movements among these routes are optimized simultaneously. To ensure the feasibility of optimized solutions for an entire operational day, the sequence and separation requirements for aircraft on runways and along selected routes are included in this second phase. In order to address these issues, three novel techniques are developed and added to a previously developed multilevel optimization framework, *viz.*, a runway assignment model, a conflict detection algorithm, and a rerouting technique. The proposed framework is applied to a realistic case study at Amsterdam Airport Schiphol in the Netherlands, in which 599 departure flights and 13 different SIDs are considered. The optimization results show that the proposed model can offer conflict-free solutions, one of which can lead to a reduction in the number of people annoyed of up to 21%, and a reduction in fuel consumption of 8% relative to the reference case solution.

Keywords: trajectory optimization; aircraft allocation; aircraft noise; airport noise; aircraft separation; conflict detection.

1. Introduction

Air transport is predicted to rapidly increase in the coming years due to its social and economic benefits (Boeing, 2016). The increase in air traffic volume may bring certain advantages to the development of society such as job creation, tourism, and industrial globalization. However, it also causes negative impacts on the quality of life of communities surrounding airports, especially as a result of aircraft noise nuisance and pollutant emissions (Asensio et al., 2017). Aircraft noise has been linked to various human health effects such as cardiovascular diseases, sleep disturbance, hearing loss, communication interference, and annoyance (Janssen et al., 2014; Morrell et al., 1997). Noise impact has been well recognized as one of the most significant factors leading to restrictions on the expansion of flight and airport operations (Rodríguez-Díaz et al., 2017).

In an effort to support the sustainable development of air transport, the International Civil Aviation Organization (ICAO) has provided the guideline for air traffic management (ICAO, 2016), and various approaches have been studied and proposed over the years (Casalino et al., 2008; Filippone, 2014; Gardi et al., 2015). In order to reduce noise impact caused by aircraft departure/arrival operations, noise abatement trajectory optimization has been applied to generate optimal trajectories, and a significant reduction in both the number of people affected by aircraft noise and fuel consumption has been reported (Zaporozhets and Tokare, 1998; Braakenburg et al., 2011; Hartjes et al., 2014, 2010, 2016; Ho-Huu et al., 2017, 2018; Hogenhuis et al., 2011; Prats et al., 2011, 2010b, 2010a; Song et al., 2014; Torres et al., 2011; Visser and Wijnen, 2003, 2001; Yu et al., 2016; Zhang et al., 2018). Furthermore, the development of allocation models to distribute aircraft movements over specific routes and runways have contributed to a significant reduction of aircraft noise effects (Chatelain and Van Vyve, 2018; Frair, 1984; Ganić et al., 2018; Ho-Huu et al., 2019a; Kuiper et al., 2012; Zachary et al., 2011, 2010). In addition to the research on aircraft noise reduction, research on improving airport capacity and fuel consumption has been widely conducted (D'Ariano et al. 2015; Sama et al. 2017a, 2017b, 2018, 2019).

Although a large effort has been made towards finding suitable options to support the continued growth of air transport, there is still a lack of studies that consider different aspects of flight and airport operations concurrently. In particular, research on the design of optimal routes typically considered only one standard route at a time, while its interaction with other routes was not included, as evident from Refs. (Braakenburg et al., 2011; Hartjes et al., 2014, 2010, 2016; Ho-Huu et al., 2017, 2018; Prats et al., 2011, 2010a; Torres et al., 2011; Visser and Wijnen, 2001, 2003; Zhang et al., 2018). Although optimal routes can offer certain benefits, either in terms of noise impact or fuel burn, from an operational perspective, they might be rather difficult to apply when other factors, such as airspace capacity or aircraft separation, are not taken into account. Meanwhile, research on the allocation of aircraft to current-in-use runways and routes can provide more realistic solutions, as reported in Refs. (Chatelain and Van Vyve, 2018; Frair, 1984; Ganić et al., 2018; Kuiper et al., 2012; Zachary et al., 2011, 2010). However, these studies relied on the assumption that the optimal solutions satisfy operational requirements, such as aircraft sequence and separation. Therefore, the true influence of optimal allocation solutions on these issues has not yet adequately studied. Moreover, since these models only considered standard routes instead of optimized routes, the potential noise and fuel reduction benefits were not fully exploited. As a result, there is a need for the development of methodologies that can exploit the advantages of these two types of problems by considering them simultaneously or in a linked manner.

In recent work (Ho-Huu et al., 2019b), a two-step optimization framework was developed that can partly deal with the combination of the above two problems. Owing to the advantages inherited from the combination of optimal route design and the distribution of flights among these routes, the two-step framework revealed the potential to considerably reduce the number of people annoyed and fuel consumption. Furthermore, the study indicated that the application of the two-step approach can help to significantly reduce the complexity of the combined problem, while keeping the quality of solutions at almost the same level as in the fully integrated (one-step) approach. Also, the framework proved to be substantially more efficient in terms of the computational cost and flexibility to adapt to changes in the flight schedules. However, since this research mainly focused on the development and validation of an appropriate approach to cope with the complexity of the combined problem, some other operations-related issues were simplified. Specifically, the capacity limits of routes and runways in the framework were implicitly assumed to be satisfied by enforcing a constraint that limits the number of aircraft movements on each route. Moreover, because the sequence and separation requirements for flights were essentially ignored, the results found were just simple distribution solutions that do not contain any information on individual aircraft movements, such as departure times.

As a continued development of the previous work, this paper proposes additional techniques and integrates them into the previous model to help overcome the above-mentioned research gaps. Similar to the previous model, the newly proposed framework also features two consecutive steps, in which Step 1 addresses the design of optimal routes, whilst Step 2 copes with the selection of routes and the distribution of flights among selected routes. Since the main research gaps of the previous work relate to Step 2, the problem model in Step 1 remains unchanged. In contrast, the optimization model in Step 2 has been reformulated as a result of the introduction of new constraints on the throughput capacity of runways and routes. In order to handle these new constraints, three new tool components are proposed. The first one is the development of a runway assignment model that is used to make sure that the safe separation requirements for all aircraft on runways are satisfied. The second additional component concerns a conflict detection algorithm that is included to check the separation requirements between aircraft along selected routes. Finally, a rerouting technique is proposed to resolve any separation violation between aircraft along the selected routes that still might exist after the conflict detection algorithm has been applied.

The proposed framework is demonstrated through a realistic case study at Amsterdam Airport Schiphol (denoted as AMS), in which a full operational day involving 599 fights and 13 different given standard instrument departure routes are considered. The obtained results are then analyzed and compared with those obtained from the reference case.

The remainder of the paper is organized as follows. Section 2 provides a brief introduction of the problem statement. Section 3 presents the proposed framework in detail, including a reformulated two-step optimization approach, a runway assignment model, a conflict detection algorithm, and a rerouting technique. Section 4 provides brief information on the optimization techniques that are used to solve optimization problems in the framework. The application of the proposed framework for a case study at AMS is presented in Section 5. Finally, conclusions are drawn in Section 6.

2. Problem statement

Before discussing the functioning of the proposed framework, an example of a representative problem at a generic airport is presented first. Fig. 1 shows a hypothetical example of four Standard Instrument Departure (SID) routes (hereafter referred to as SIDs[†]) and the surrounding communities near an airport. Since noise caused by aircraft operations has significantly negative influences on the quality of life of communities surrounding the airport (in particular, those located near or underneath the routes), the design and selection of routes for each given SID (i.e., Question 1) should be made such as to avoid as many (highly) populated areas as possible. In addition, due to the accumulative nature of noise impact, the distribution of aircraft movements among these routes while guaranteeing aircraft sequence and separation requirements (i.e., Questions 2 and 3) is also an important factor that needs to be considered. Therefore, from a noise perspective, it is apparent that the design and use of noise-optimized routes and the optimal distribution of aircraft movements among these routes emerge as appropriate options that can help to reduce the aircraft noise impact on communities around the airport. However, due to the intricate coupling that exists between these two problems and the associated high computational cost, it is challenging to solve these problems integrally in a single step.

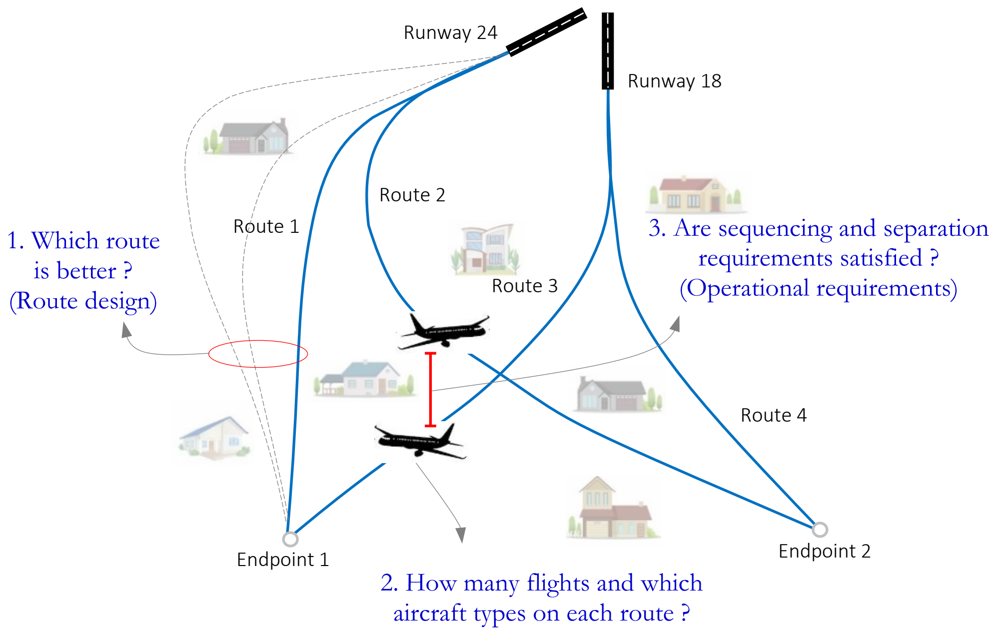

Fig. 1. An example of routes and communities around an airport.

[†] Please note that the notation of SID is used to denote an existing published Standard Instrument Departure route that connects a given runway to a defined terminal endpoint, while "routes" are used in the context of this paper to represent the optimized ground tracks that are created for each SID by using an optimization algorithm.

In this work, a multilevel optimization framework is developed to overcome the complexity of the integrated problem, as well as the limitations of the computational burden. The main aim of the framework is to provide solutions that address all three questions together while minimizing the number of people affected by aircraft noise. Particularly, the final goal of the framework is to determine, for each given SID, which route is optimal, and how many movements of each aircraft type should be assigned to this route while taking aircraft sequence and separation requirements into account. Nevertheless, purely focusing on noise impact may lead to an increase in fuel burn as a result of aircraft seeking to circumnavigate populated areas. Therefore, fuel consumption is included as a second objective function in the formulation of the optimization problem. The two objectives are briefly described below.

To determine the Number of People Annoyed (hereafter defined as NPA), the L_{den}-based annoyance criterion, proposed by EEA (2010), is applied in this study. According to EEA (2010), the percentage of People Annoyed (%PA) at a given location on the ground is defined as

$$\%PA = 8.588\times10^{-6}(L_{\mathrm{den}}-37)^3 + 1.777\times10^{-2}(L_{\mathrm{den}}-37)^2 + 1.221\,(L_{\mathrm{den}}-37) \tag{1}$$

where L_{den} is the day-evening-night noise level, determined by

$$L_{\mathrm{den}} = 10\log_{10}\left[\sum_{k\in N_{\mathrm{r}}}\sum_{i\in N_{\mathrm{at}}}\sum_{j\in O_{\mathrm{t}}} a_{ikj}10^{\frac{SEL_{ik}+w_{\mathrm{den},j}}{10}}\right] - 10\log_{10}T \text{ (dBA)}, \tag{2}$$

where N_{r} is the total number of given SIDs; N_{at} is the total number of aircraft types; O_{t} is the operational time, which includes day, evening and night time; SEL_{ik} is the sound exposure level caused by aircraft type i on route k; $w_{\mathrm{den},j}$ is a penalty weighting factor, which is either of 0, 5, or 10 dBA, accounting for day, evening and night time operations, respectively; a_{ikj} is the number of aircraft type i operating on route k at the time period j; and T is the considered period of time in seconds (T = 24×3600 seconds in this case). In Eq. (2), the SEL metric is computed at each location on the ground by using a replication of the noise model laid down in the technical manual of ECAC (2016).

The fuel objective is determined as

$$T_{\mathrm{fuel}} = \sum_{k\in N_{\mathrm{r}}}\sum_{i\in N_{\mathrm{at}}} a_{ik}\, fuel_{ik} \tag{3}$$

where $fuel_{ik}$ is the fuel that aircraft type i consumes when operating on route k. The $fuel_{ik}$ is calculated by using an intermediate point-mass model (Hartjes et al., 2016) and the Base of Aircraft DAta (BADA) (EUROCONTROL, 2014b).

3. A multilevel optimization framework

In this section, the proposed multilevel optimization framework is presented in detail. The flowchart of the framework is illustrated in Fig. 2, while a description of the details will be given in the following subsections.

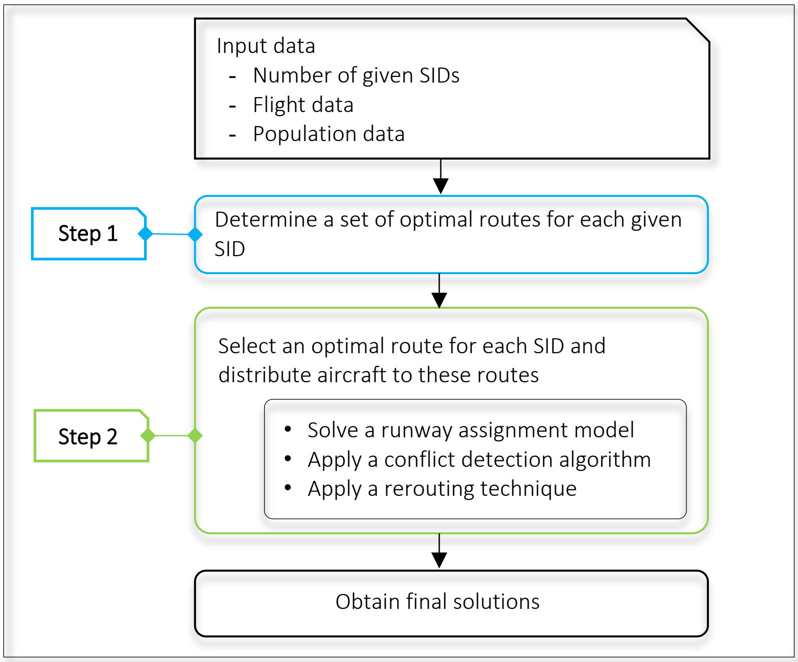

Fig. 2. Flowchart of the multilevel optimization framework.

3.1. A two-step approach

3.1.1. Step 1: design of optimal routes

In order to generate, for each given SID, a set of optimal routes that effectively balances between NPA and fuel burn, a multi-objective trajectory optimization problem is formulated and solved. The optimization problem is defined as

$$\min_{\mathbf{p}} \quad \left(N_{\text{pa}}(\mathbf{p}), T_{\text{fuel}}(\mathbf{p})\right) \tag{4}$$

$$\text{s.t.} \quad \mu_i(t) \le \mu_{\max}(h), \quad \forall i \in N_{\text{at}} \tag{5}$$

where $N_{pa}(\mathbf{p})$ is the total NPA, and $T_{fuel}(\mathbf{p})$ is the total fuel consumption of all aircraft following the SID. The design variables are the parameters that define a route; these parameters are collected in the vector **p**. For more details about the definition of the vector **p**, interested readers can refer to Ho-Huu et al. (2017; 2019b). The variable $\mu_i(t)$ in Eq.(5) is the bank angle of aircraft type i during a turn at time t, and μ_{max} is the maximum permissible value of μ, varying according to altitude h (ICAO, 2006).

In Eq. (4), the objective $N_{pa}(\mathbf{p})$ is calculated by considering the multiplication of $\%PA$ in Eq. (1) in each grid cell with the population in that cell and subsequent aggregation over all cells. The population density data surrounding an airport is retrieved from a Geographic Information System (GIS). The objective $T_{fuel}(\mathbf{p})$ in Eq. (4) is defined similarly as in Eq. (3). It is noted that N_r is now by default equal to 1 since only one SID at a time is evaluated.

The optimization problem is applied for all considered SIDs. The obtained sets of optimal routes and their associated performances for all SIDs are then utilized as inputs for the optimization problem in Step 2. It should be noted that to be able to adapt to different runway configurations, the optimal routes for all given SIDs originating from each runway should be obtained.

3.1.2. Step 2: selection of routes and distribution of flight among these routes

Before going to the formulation of an optimization problem, it is assumed that the terminal point for each flight listed in the flight schedule is assumed to be specified in advance, based on its destination airport. From the sets of optimal routes obtained in Step 1, this step aims to determine, for each given SID, which route from the set should be selected, as well as to determine how many movements of each aircraft type should be assigned to this route for an entire day. The formulation of the flight distribution optimization problem is mathematically formulated as follows.

$$\min_{\mathbf{a},\mathbf{r}} \quad \left(N_{pa}(\mathbf{a},\mathbf{r}), T_{fuel}(\mathbf{a},\mathbf{r})\right) \tag{6}$$

$$\text{s.t.} \quad \sum_{k \in SD_s} a_{ik} = T_{a,is}, \quad \forall i \in N_{at}, \forall s \in T_p \tag{7}$$

$$f_d(\mathbf{a},\mathbf{r}) = 0 \tag{8}$$

$$f_{sr}(\mathbf{a},\mathbf{r}) \le 0 \tag{9}$$

$$0 \le a_{ik} \le \bar{a}_{ik}, \forall k \in SD_s, \forall i \in N_{at} \tag{10}$$

where $\mathbf{a}$ is the design variable vector of flight distribution, in which a_{ik} is the number of aircraft type i on route k. The vector $\mathbf{r} = \{r_1,.., r_k..., r_{Nr}\}$ is the design variable vector of route selection, where the preferred route r_k is chosen from the set of optimal routes $\mathbf{O}_k$ obtained in Step 1 for SID k. The index s relates to the terminal point (defined as the endpoint of each departure procedure), and T_p is the set of terminal points, $s \in T_p$. The vector SD_s is the vector that collects the SIDs which share the same terminal point s. The parameter $T_{a,is}$ is the total number of aircraft type i assigned to SIDs having the same terminal point s. Eq. (10) represents the set of boundary constraints on the design variables, where the parameter $\bar{a}_{ik}$ is the upper bound of the number of aircraft type i on route k, and it can be extracted from the flight schedule as the total number of aircraft type i assigned to SIDs having the same terminal point. The function $f_d(\mathbf{a},\mathbf{r})$ is a constraint imposing the separation requirements between aircraft on the runways and is defined in the runway assignment model presented in Section 3.2. Similarly, the function $f_{sr}(\mathbf{a},\mathbf{r})$ is related to safeguarding the separation requirements between aircraft along the selected routes and is defined in the conflict detection algorithm presented in Section 3.3.

In the above optimization problem (Eqs. (6-10)), the objectives $N_{pa}(\mathbf{a},\mathbf{r})$ and $T_{fuel}(\mathbf{a},\mathbf{r})$ are defined in a similar fashion as in Step 1. However, the design variables considered here are different. Particularly, the design variables in this step represent the routes selected from the sets of available optimal routes for each SID, and the distribution of flight among these routes. Meanwhile, the design variables in Step 1 are the geometric parameters that are used to construct a SID route. Note that the two objective functions in Eq. (6) are only calculated if the constraint in Eq. (8) is satisfied; otherwise, large numbers are assigned to the criteria, representing penalties on an infeasible solution. This avoids the computationally expensive calculation of the objective values when infeasible solutions are considered. Also, all the information associated with routes and aircraft types is known a priori in Step 2, as this information has been stored in Step 1.

3.2. Runway assignment model

The main objective of the model is to find, for any given instance of $(\mathbf{a},\mathbf{r})$ considered in Step 2, a suitable conflict-free solution for the assignment of individual flights to specific routes and runways, while minimizing the total departure delay (relative to the departure times listed in the flight schedule) at runways. It is noted that the original objectives in Eq. (6) – NPA and fuel – are the focus of the main distribution algorithm, which determines which share of the total movements (for each aircraft type) are assigned to a specific route. In other words, the flight distribution optimization problem only considers the flows of aircraft movements. The flight to runway assignment model, on the other hand, merely determines how individual flights are assigned to runways, essentially looking for a conflict-free realization at the runways of the flow solution generated by the flight distribution optimization algorithm, taking departure times into account. Therefore, the flight to runway assignment has no impact on the original objectives NPA and fuel. It is important to note that although the runway assignment model yields solutions that are free of conflict at the departure runway, separation conflicts might still occur down-route. The handling of potential down-route conflicts is discussed in Section 3.3. It is also important to note that when a flight is assigned to a runway, its route is automatically determined. The flight to runway assignment model is mathematically written as follows.

$$\min_{\mathbf{x},\mathbf{d}} \quad \sum_{j\in J} d_j \tag{11}$$

$$\text{s.t} \quad (t_{j+1}+d_{j+1})-(t_j+d_j)-Mx_{j+1}^r-Mx_j^r \geq t_s-2M, \forall j\in J, \forall r\in R \tag{12}$$

$$(t_{j+1}+d_{j+1}) \geq (t_j+d_j), \forall j\in J \tag{13}$$

$$\sum_{r\in R} x_j^r = 1, \ \forall j\in J \tag{14}$$

$$\sum_{j\in J} c_{jis} x_j^r = N_{is}^r, \ \forall i\in N_{\mathrm{at}}, \forall s\in T_{\mathrm{p}}, \forall r\in R \tag{15}$$

where **x** is the vector of binary design variables x_j^r, in which x_j^r represents the assignment of flight j to runway r, $x_j^r \in \{0,1\}$. The vector **d** is the vector of delay variables d_j, where d_j ($d_j \geq 0$) represents the departure delay of flight j at the runway. The parameters J and R are, respectively, the set of flights in the flight schedule and the set of runways. The parameter t_j is the scheduled departure time of flight j, and t_s is the required time separation, which depends on the weight classes of following and leading aircraft, as indicated in EUROCONTROL (2018) (see Table 1). Note that the empty fields in Table 1 indicate a minimum departure interval of 60 seconds (Delsen, 2016). The parameter c_{jis} is the constraint coefficient of flight j that is associated with aircraft type i and terminal point s. The coefficient c_{jis} will be equal to 1 if flight *j* of aircraft type *i* flies to terminal point *s*, otherwise it will be equal to 0. The parameter N_{is}^{r} is the total number of aircraft type *i* departing from runway *r* to terminal point *s*. It is noted that, for any instance of (**a**,**r**) produced by the aircraft distribution optimization algorithm, the parameters N_{is}^{r} can be determined up front from the flight schedule information.

Table 1. RECAT-EU wake turbulence time-based separation minima on departure (EUROCONTROL, 2018).

RECAT-EU scheme		“Super Heavy“	“Upper Heavy”	“Lower Heavy”	“Upper Medium”	“Lower Medium”	“Light”
Leader / Follower		“A”	“B”	“C”	“D”	“E”	“F”
“Super Heavy”	“A”		**100s**	**120s**	**140s**	**160s**	**180s**
“Upper Heavy”	“B”				**100s**	**120s**	**140s**
“Lower Heavy”	“C”				**80s**	**100s**	**120s**
“Upper Medium”	“D”						**120s**
“Lower Medium”	“E”						**100s**
“Light”	“F”						**80s**

In the optimization problem (Eqs. (11-15)), the objective function represents the minimization of the total departure delay. The first constraint aims to ensure that the separation requirement between two consecutive aircraft on the same runway is always satisfied. The parameter *M* in the constraint is a large number (e.g., 10^6) that helps to render the constraint inactive in the case that two consecutive aircraft are assigned to two different runways. For example, if two consecutive aircraft are assigned to two different runways (i.e., x_j^r = 1 and x_{j+1}^r = 0 or x_j^r = 0 and x_{j+1}^r = 1), and the separation time between them is smaller than t_s, the constraint is still satisfied, which can be readily inferred from Eq. (12). In contrast, if two consecutive aircraft are assigned to the same runway, the separation between them has to be larger than t_s; otherwise, the allocation solution is infeasible. The second constraint Eq. (13) ensures that the sequence of flights listed in the flight schedule is kept unchanged when departure delays are introduced. The third constraint guarantees that each flight is assigned to one runway only. Finally, the last constraint aims to ensure that the assignment of aircraft on each runway always matches the information of the distribution variables in the main optimization problem in Step 2 and complies with the flight information and aircraft sequence as given in the flight schedule.

In order to determine the constraint Eq. (8) in Step 2, the function $f_d(\mathbf{a},\mathbf{r})$ is defined as

$$f_{\mathrm{d}}(\mathbf{a},\mathbf{r}) = \sum_{j \in J} d_j - \overline{\mathrm{D}} \tag{16}$$

where $\overline{\mathrm{D}}$ is the total delay at the runways, which is derived from the runway assignment problem without considering the distribution constraint Eq. (15). Therefore, the delay $\overline{\mathrm{D}}$ is independent from the solution $(\mathbf{r},\mathbf{a})$ and can be calculated up front by solving the optimization problem in Eqs. (11-14) based on a given flight schedule and set of available runways. Meanwhile, the delay $\sum d_j$ in Eq. (16) associated to a solution instance $(\mathbf{r},\mathbf{a})$ might be influenced by the inclusion of the constraint Eq. (15). Since the problem in Eqs. (11-14) represents a relaxation of the problem in Eqs. (11-15), the value of $\overline{\mathrm{D}}$ will not exceed that of $\sum d_j$. Therefore, the constraint $f_d(\mathbf{a},\mathbf{r}) = 0$ enforced in Eq.(8) makes sure that the solutions obtained by the optimization problem in Step 2 do not cause a delay compared with the delay $\overline{\mathrm{D}}$, and hence the runway capacity is kept at the maximum level.

3.3. Conflict detection algorithm

Once the result of the runway assignment model has been returned, an additional check is carried out with respect to the satisfaction of constraint Eq. (9) along the routes. If the returned result does not satisfy the delay constraint Eq. (8), the check is no longer needed, and a large penalty number is assigned to this constraint. Otherwise, a conflict detection algorithm will be evoked to check the separation requirement of aircraft along the selected routes.

From the flight schedule and the assignment solution returned by the assignment model, the route information and associated performance can be obtained for each flight. This information comprises the flight trajectory (i.e., position coordinates, velocity, altitude, time), fuel burn and noise value (i.e., SEL). After the trajectories for all flights in the flight schedule have been defined, a simulation process is carried out for all flights contained in the schedule, using an iteration time step of 10 seconds (as suggested by Isaacson and Erzberger (1997)). In order to check the aircraft separation requirements in both vertical and horizontal dimensions, the distance separation minima suggested by ICAO (2016) and

EUROCONTROL (2018) is applied. The vertical separation is set to 1,000 ft (ICAO, 2016), while the horizontal separation standards are given in Table 2 (EUROCONTROL, 2018). The horizontal separation is defined here as the Euclidean distance in the horizontal plane between the aircraft in each pair (Isaacson and Erzberger, 1997; Visser, 2008). It is noted that the separation minima indicated in Table 2 are applied to flights operating on the same routes, while for those operating on different routes, a minimum radar separation of 3 NM is enforced. It should also be noted that only the wake vortex separation minima are enforced and that all runways are assumed to be operated independently, i.e., departures can take place simultaneously at all runways. The main procedure of the algorithm is described in Algorithm 1.

Table 2. RECAT-EU wake turbulence distance-based separation minima on approach and departure. (EUROCONTROL, 2018).

RECAT-EU scheme		“Super Heavy“	“Upper Heavy”	“Lower Heavy”	“Upper Medium”	“Lower Medium”	“Light”
Leader / Follower		“A”	“B”	“C”	“D”	“E”	“F”
“Super Heavy”	“A”	**3 NM**	**4 NM**	**5 NM**	**5 NM**	**6 NM**	**8 NM**
“Upper Heavy”	“B”		**3 NM**	**4 NM**	**4 NM**	**5 NM**	**7 NM**
“Lower Heavy”	“C”		**(*)**	**3 NM**	**3 NM**	**4 NM**	**6 NM**
“Upper Medium”	“D”						**5 NM**
“Lower Medium”	“E”						**4 NM**
“Light”	“F”						**3 NM**

(*) means minimum radar separation (MRS), set at 2.5 nautical mile (NM), is applicable as per current ICAO doc 4444 provisions.

Algorithm 1. Conflict detection algorithm.

```
Input:
 - Flight data;
 - Route trajectories;
 - Time step; starting time, ending time;
 - Set the couple of flights violating the required distance separation (VS) to 0, VS = 0;
For each time step
        Define flights entering into the time window;
        Extract the flight trajectories for these flights;
        Calculate the vertical distance for each couple of flights;
        For each couple of flight
              If the vertical separation is violated
                    Calculate the horizontal distance
                    If the horizontal separation is violated
                         Set VS = VS + 1;
                    End
              End
        End
End
Output: A set of couple of flights violating the required separation, VS.
```

Once the algorithm has terminated, the number of instances of flights violating the required distance separation standards is stored in the parameter *VS*. If *VS* is equal to 0, the constraint in Eq. (9) is satisfied, and hence the allocation solution is feasible. Otherwise, the allocation solution is infeasible.

It should be noted that the resolution of the runway assignment problem in Section 3.2 may lead to a situation in which multiple (non-unique) optimal solutions are found. Since the assignments of aircraft on runways for the various optimal solutions may lead to different conflict situations down-route, the conflict algorithm will be applied for each optimal solution obtained by the runway assignment model. Subsequently, the solution without any conflicts or that with the smallest number of conflict cases is selected. In the latter case, the rerouting technique will be subsequently applied to the identified conflicting flights and will be presented in detail in the following section.

3.4. Rerouting technique

The conflict detection algorithm is applied to every distribution solution obtained for the optimization problem in Eqs. (6-10). If any couple of flights in these solutions violate separation minima which is discovered by the conflict detection algorithm, a rerouting technique is used. The idea behind the rerouting method is similar to that of the vectoring solutions as currently issued by Air Traffic Controllers (ATC), which is used to resolve the conflict between flights listed in the schedule when they fly along the selected routes. In the rerouting method, alternative routes are assigned to each pair of flights whose separation distances violate the specified minima while still optimizing noise impact and fuel consumption. To this end, an optimization problem is formulated and solved for each pair of conflicting flights in the flight distribution solution. The associated optimization problem is written as follows.

$$\min_{\mathbf{r}_{ac}} \quad w_1 \frac{N_{pa}(\mathbf{r}_{ac})}{N_{pa}(\mathbf{a},\mathbf{r})} + w_2 \frac{T_{fuel}(\mathbf{r}_{ac})}{T_{fuel}(\mathbf{a},\mathbf{r})} \tag{17}$$

$$\text{s.t.} \quad f_{sr}(\mathbf{r}) = 0 \tag{18}$$

where $\mathbf{r}_{ac}$ is the design variable vector of alternative routes for the pair of conflicting flights whose separation violates the separation standard; the alternative routes are again selected from the sets of optimal routes obtained in Step 1. The objective function is the normalization of the NPA and fuel consumption, in which $N_{pa}(\mathbf{r}_{ac})$ and $T_{fuel}(\mathbf{r}_{ac})$ are the NPA and the total fuel burn associated with new alternative routes for conflicting flights, respectively; and $N_{pa}(\mathbf{a},\mathbf{r})$ and $T_{fuel}(\mathbf{a},\mathbf{r})$ are, respectively, the NPA and the total fuel burn associated with the design variables of the optimization problem in Eqs. (6-10). Note that $N_{pa}(\mathbf{a},\mathbf{r})$ and $T_{fuel}(\mathbf{a},\mathbf{r})$ are known at this stage. The parameters w_1 and w_2 are the weighting factors, which are used to transfer a bi-objective optimization problem into a single objective one. In this case, w_1 and w_2 are set to 0.5 with the aim of giving an equal priority to both the NPA and fuel consumption. This setting also aims to retain the diversity of solutions in the original Pareto front. As illustrated in Fig. 3, due to the use of the equivalent weight of 0.5 for both objectives, the solution obtained by the optimization problem in this section is expected to be located along the dotted diagonal line, which is the line having an angle of 45 degrees relative to the horizontal axis.

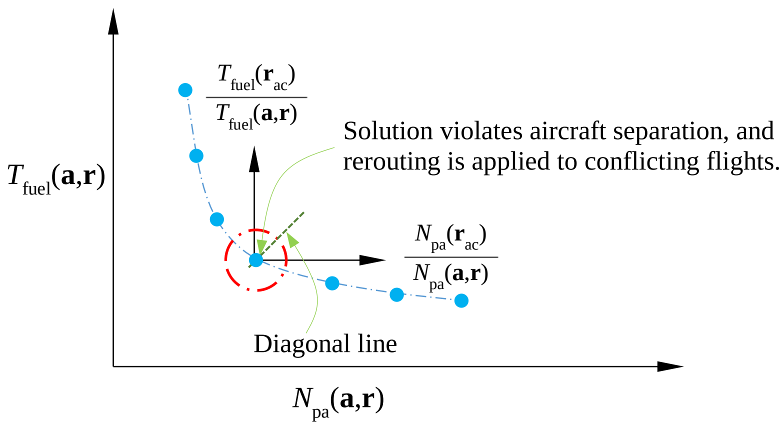

Fig. 3. Illustration of the optimal solution of the optimization problem in Eqs. (17-18).

The evaluation of the constraint is performed by evoking the conflict detection algorithm in Section 3.3. In this case, however, only flights involved in a time interval, within which conflict between flights take place, are taken into account. The time interval is determined by the total travel time of the pair of conflicting flights from the runways to the endpoints. To make sure the selection of new routes for the conflicting flights do not cause any conflicts to other flights outside of the time interval, the travel time of the conflicting flights is estimated based on the longest route stored in the set of available routes for each SID. The determination of the time interval and the identification of flights within this interval is illustrated in Fig. 4. In the figure, the two conflicting flights are f_3 and f_4; the time interval is delimited by the starting time of flight f_3 and the ending time of flight f_4; and the flights involved in this time interval are f_1, f_2, and f_5. Since only flights operating within the time interval are considered, the rerouting of conflicting flights does not influence flights outside this time interval. Furthermore, since typically only a few flights in the flight schedule are involved, the computational cost of solving the problem in this step is relatively small, just a few seconds of CPU time.

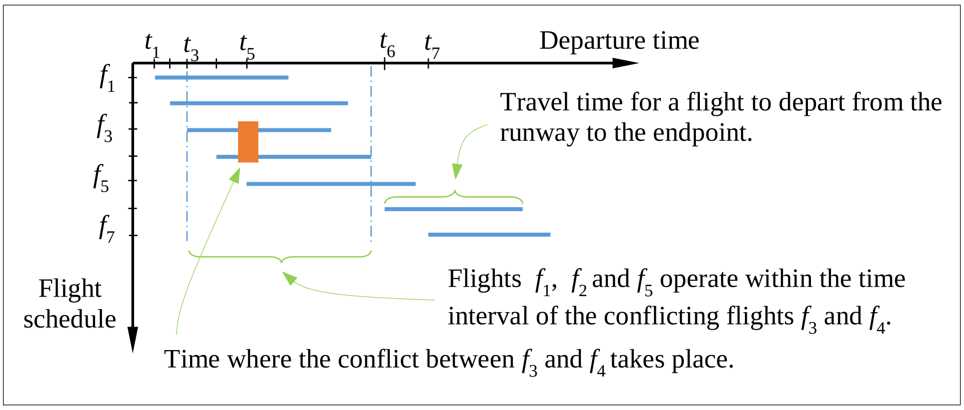

Fig. 4. Illustration of the number of flights involved in the time interval within which the conflict takes place.

When the conflict detection tool identifies more than one pair of conflicting aircraft, the rerouting algorithm is sequentially applied to each conflicting pair. Note that the rerouting technique is applied to every distribution solution obtained for the optimization problem in Eqs. (6-10) if the solution contains any couple of flights violating the separation standard.

4. Optimization techniques

As can be seen in Section 3, four different optimization problems have been established. The first two problems are nonlinear multi-objective parameter optimization problems. The third problem is a mixed integer linear programming problem (MILP) which is nested in the second problem, and the last one is a nonlinear single-objective parameter optimization problem. To solve these four problems, four different optimization methods are used. For the first problem (Eqs. (4-5)), the Multi-objective Optimization Evolutionary Algorithm based on Decomposition (MOEA/D), as proposed by Zhang and Li (2007) and improved by Ho-Huu et al. (2017), is applied. This choice is motivated by the fact that MOEA/D has been demonstrated to be an efficient method to deal with this type of problems (Ho-Huu et al., 2017). Meanwhile, the Non-dominated Sorting Genetic Algorithm (NSGA-II) (Deb et al., 2002) is utilized to solve the second problem (Eqs. (6-10)). The preference for this method is, in this case, because the design space of this problem is very restricted, and hence the solutions easily violate the constraints. Therefore, NSGA-II is more suitable than MOEA/D in this case. A mixed integer linear solver from the CPLEX optimization suite/library is applied to solve the linear optimization problem (Eqs. (11-15)). Finally, the last problem (Eq. (17-18)) is solved by using the Differential Evolution (DE) algorithm (Storn and Price, 1997). For more details on MOEA/D, NSGA-II, and DE, interested readers are referred to Refs. (Ho-Huu et al., 2017; Zhang and Li, 2007), (Storn and Price, 1997), and (Deb et al., 2002), respectively. It should be noted that, in order to deal with the equality constraint in Eq. (7), a constraint handling technique developed in (Ho-Huu et al., 2018) has been applied and coupled to the NSGA-II algorithm. Please note that since some of the applied optimization methods, including MOEA/D, NSGA-II and DE, are heuristic methods, the solutions obtained by these methods are only approximate or nearly optimal solutions. As a consequence, the word "optimized" is used in the later section instead of "optimal" to express the obtained solutions when the above-mentioned optimization techniques are applied to solve the optimization problems.

5. Numerical results and discussion

In this section, the reliability and efficiency of the proposed framework are evaluated using a realistic case study at Amsterdam Airport Schiphol (denoted as AMS) in The Netherlands. On the selected reference day, 599 departure flights were recorded, that operated on two runways, *viz.*, RWs 24 and 18L (Dons, 2012), as shown in Fig. 5.

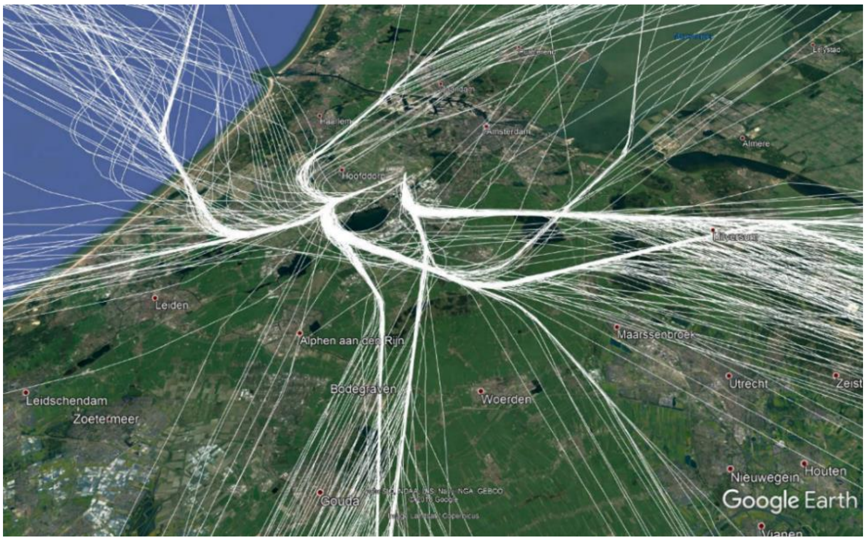

Fig. 5. Illustration of real departure operations at AMS.

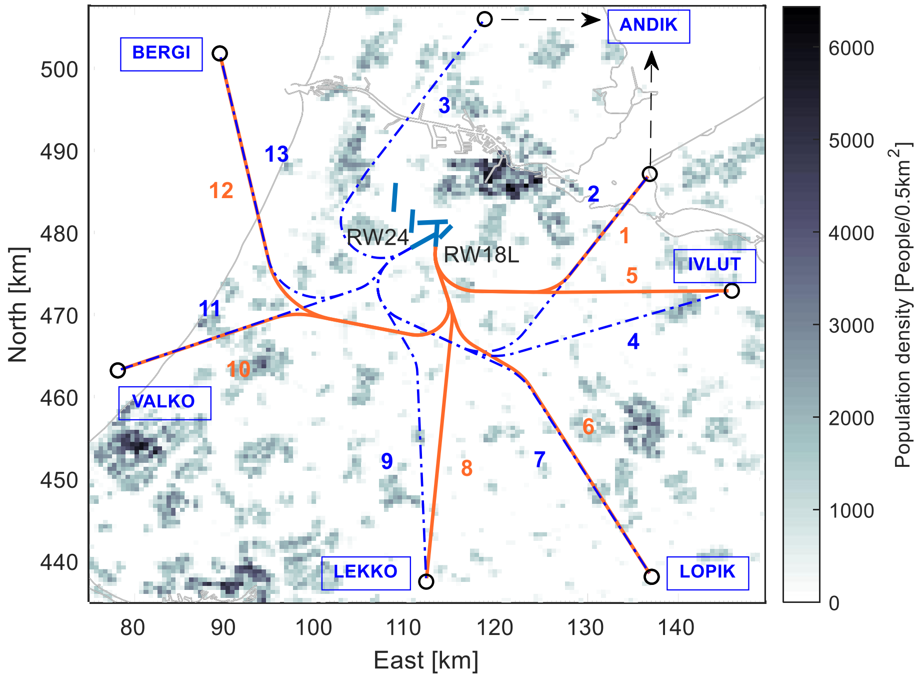

Fig. 6. Illustration of departure routes at AMS.

According to the flight data and the Aeronautical Information Publication (AIP)[‡], 13 distinct SIDs were in use on the reference day, as shown in Fig. 6. In the figure, the solid routes originating from RW18L are highlighted and numbered in orange, while the dashed routes originating from RW24 are highlighted and numbered in blue. There are 6 terminal points (defined as the endpoints of departure procedures in this study), *viz*. ANDIK, IVLUT, LOPIK, LEKKO, VALKO and BERGI. Each terminal point is connected by two routes originating from either RW24 or RW18L, except for ANDIK that is connected by three routes, consisting of route 1 from RW18L and routes 2 and 3 from RW24. Note that, from the assignment solution produced by the runway assignment model, the assignment of flights to routes for the terminal points IVLUT, LOPIK, LEKKO, VALKO, and BERGI is automatically known, as there is only a single route available from each runway.

However, for the terminal point ANDIK, two different routes are available from RW24 runway, and hence an additional step is needed. To determine which flight is assigned to either route 2 or 3 from RW24, the following heuristic rule is applied. In order to reduce the number of potential crossing conflicts between flights during the peak hours, flights operating in this time period are assigned to route 3 until its capacity limit is reached; the remainder of the flights are assigned to route 2.

Though many different aircraft types operate on these routes, for the sake of simplicity, all flight movements are represented here by either of three aircraft types, namely, Fokker 100 (F100), Boeing 737-800 (B738), and Boeing 777-300 (B773). It is assumed that the F100, B738, and B773, respectively, represent lower medium (LM), upper medium (UM) and upper heavy (UH) aircraft, as classified by EUROCONTROL (2015). The population data provided by the Dutch Central Bureau of Statistics (CBS) (Centraal Bureau voor de Statestiek) with a grid cell size of 500 x 500 m, as shown in Fig. 6, is used. The detailed data of aircraft movements is provided in Table 3. All the simulations are carried out in MATLAB 2018b on an Intel Core i5 and 8GB RAM desktop.

Table 3. The detailed data for aircraft operations.

Terminal point	Number of aircraft movements			
	Entire day [LM, UM, UH]	Day (7h00-19h00) [LM, UM, UH]	Evening (19h00-23h00) [LM, UM, UH]	Night (23h00-7h00) [LM, UM, UH]
ANDIK	[45, 22, 8]	[32, 14, 3]	[6, 6, 5]	[7, 2, 0]
IVLUT	[74, 98, 43]	[57, 69, 28]	[9, 10, 12]	[8, 19, 3]
LOPIK	[7, 11, 2]	[4, 9, 2]	[2, 1, 0]	[1, 1, 0]
LEKKO	[35, 76, 3]	[30, 46, 3]	[3, 8, 0]	[2, 22, 0]

‡ https://www.lvnl.nl/eaip/2019-12-19-AIRAC/html/index-en-GB.html (accessed 2 January 2020).

VALKO	[36, 31, 12]	[27, 24, 10]	[4, 4, 1]	[5, 3, 1]
BERGI	[34, 26, 36]	[27, 18, 35]	[4, 7, 0]	[3, 1, 1]
Total	[231, 264, 104]	[177, 180, 81]	[28, 36, 18]	[26, 48, 5]

5.1. Evaluation of the distribution model in Step 2

Since the aircraft sequence and separation requirements are considered and integrated into the distribution model in Step 2, it is important to investigate the performance of this model independently. The main aim of this investigation is to see whether, based on the current SIDs, the model can provide better distribution options to reduce noise impact and fuel consumption compared with the reference case.

Before executing the model, the reference case is determined first. The reference case considers the 599 flights, as shown in Fig. 5. It is noted that due to capacity reasons, the flights in Fig. 5 have been vectored by Air Traffic Controllers (ATC). In order to make the calculation of the reference case simpler, it is assumed here that all vectored flights are simply assigned to one of the fixed routes as shown in Fig. 6. By recreating the traffic flow based on the reference data (which include the actual departure times) and the standard routes as defined in Fig. 6, the number of people annoyed and the total fuel burn in ton are 75,800 and 332.20, respectively, and there is no delay at the runways, i.e., $\overline{\mathrm{D}} = 0$. The result also shows that 8 cases of flights which violate the required separation minima emerge. Nevertheless, the number of conflicting flights remains small, representing less than 2% of the total traffic volume. For comparison purposes, therefore, it is assumed that all distribution solutions derived from the distribution model are deemed acceptable if they feature less than 8 violations.

To solve the problem defined by Eqs. (6-10), the NSGA-II algorithm with a population size of 70 and a maximum number of 1500 generations (Gen.), as used in Ho-Huu et al. (2019a), is applied. Fig. 7 shows the optimized results obtained by the distribution model and the solution to the reference case. As expected, it can be seen from Fig. 7 that all the solutions from the model dominate that of the reference case and are much better in both the NPA and fuel consumption. In addition, only 7 violations are recorded for solutions obtained by the proposed model, which is one case less compared with that of the reference scenario. Note that in this section the rerouting technique is not yet applied.

Regarding the performance of the optimization algorithm, it can be seen from Fig. 8 that the algorithm has a good convergence rate. After 1200 generations, the solutions start to converge, and there are no significant changes after 1300 generations. The total time for the algorithm to reach the final generation is 7.39 hours. It should be noted that because the flight schedule can be obtained some days in advance, the model can be used as a planning tool to deliver reasonable solutions for the assignment of flights a priori. Furthermore, owing to the independent evaluation of objective functions in the optimization algorithm, the computational cost of the distribution problem can be further improved by using parallel computing with multiple cores or cluster computing.

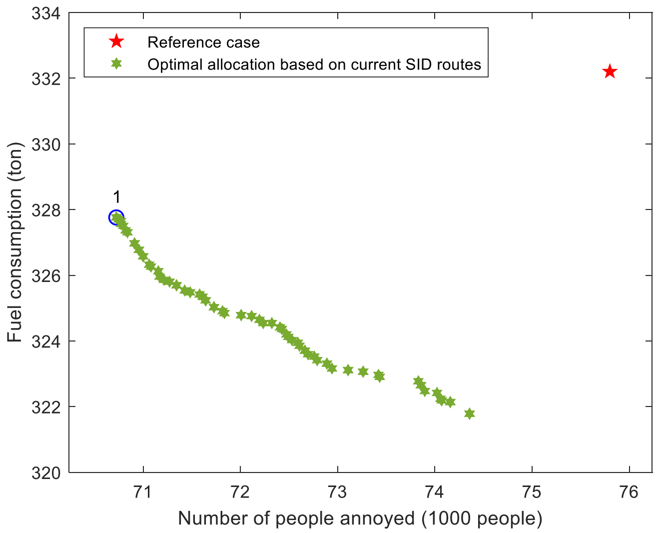

Fig. 7. Comparison of the NPA and fuel consumption obtained for the reference case and the optimized distribution solutions based on the current SID routes.

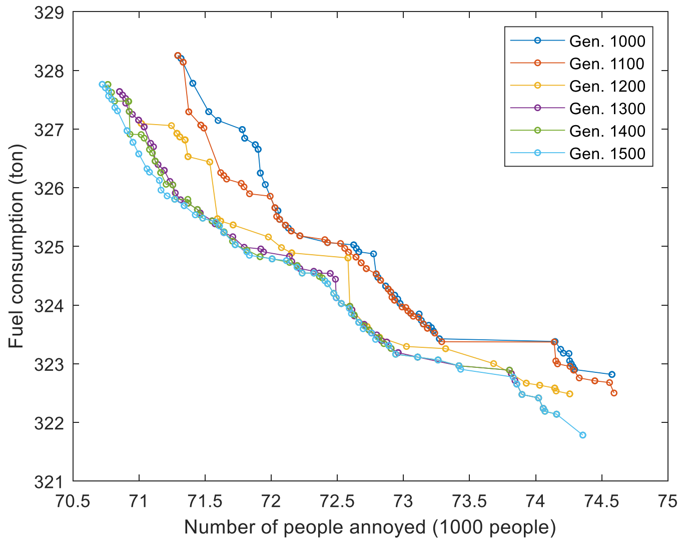

Fig. 8. Convergence history of the optimized distribution solutions based on the current SID routes.

To further examine the advantage of the model, a single representative solution, i.e., solution 1 as highlighted in Fig. 7, is selected for further analyses. The L_{den} noise contours associated to this solution are illustrated in Fig. 9, along with those resulting from the reference case. As can be seen from the figure, there is a distinct difference in the size of the L_{den} contours between the two solutions. Indeed, the contours associated with solution 1 appear to avoid populated regions better than those associated to the reference case, hence leading to a reduction in the NPA.

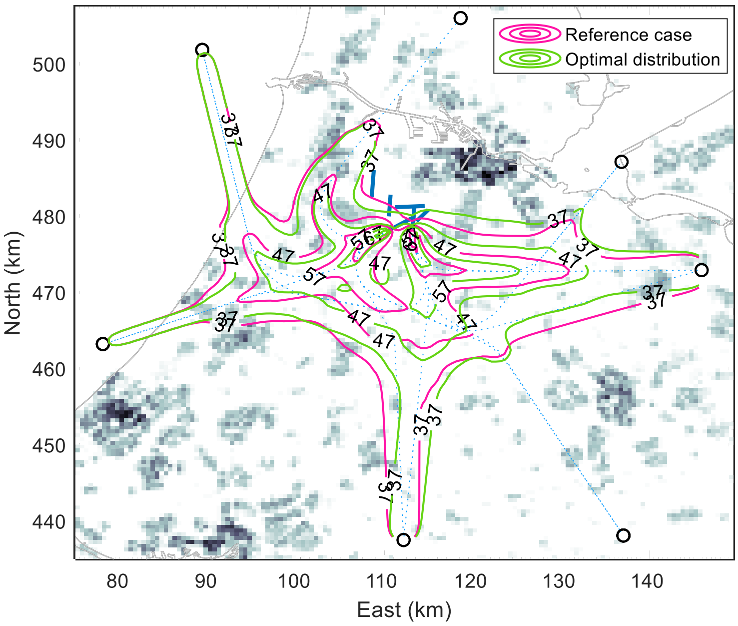

[Fig. 9]. Comparison of the L_{den} noise contours caused by the reference case and the optimized distribution solution (solution 1) based on current SIDs.

To provide a better understanding of the reason leading to the change of the contours in Fig. 9, the distribution of flights among the routes obtained in solution 1 is also provided numerically in Table 4. At first glance, it can be noted in Table 4 that there is a large shift of aircraft movements between routes 8 and 9. Specifically, on route 8 in the reference case, there are 44 daytime flights (21 F100s, 20 B738s and 3 B773s), 11 evening flights (3 F100 and 8 B738s), and no night flights, whilst in solution 1 there are 74 daytime flights (27 F100s, 44 B738s and 3 B773s), 10 evening flights (2 F100s and 8 B738s), and up to 24 night flights (2 F100s and 22 B738s). This redistribution of movements explains why in Fig. 9 the contours shift to the right of routes 8 and 9, which, evidently, results in a reduction in the NPA. Moreover, since the track along route 8 is shorter than that of route 9, more aircraft are assigned to route 8, and more fuel can be saved. The same situation can also be observed in the distribution of flights among routes 4 and 5, contributing to a significant reduction in fuel burn as a result of aircraft flying on a shorter route.

Table 4. Comparison of flight distribution obtained by the reference case and the optimized distribution solution (solution 1) based on current SIDs.

Route number	Approach	Day			Evening			Night		
		F100	B738	B773	F100	B738	B773	F100	B738	B773
1	RC*	0	0	0	2	2	2	0	0	0
	OD#	11	10	2	2	4	3	7	2	0
2	RC	3	5	2	0	1	1	7	2	0
	OD	0	0	0	0	0	0	0	0	0
3	RC	29	9	1	4	3	2	0	0	0
	OA	21	4	1	4	2	2	0	0	0
4	RC	20	31	15	1	2	1	8	19	3

	OD	3	2	3	0	0	3	0	0	0
5	RC	37	38	13	8	8	11	0	0	0
	OD	54	67	25	9	10	9	8	19	3
6	RC	3	6	0	2	1	0	0	0	0
	OD	3	9	2	2	1	0	1	1	0
7	RC	1	3	2	0	0	0	1	1	0
	OD	1	0	0	0	0	0	0	0	0
8	RC	21	20	3	3	8	0	0	0	0
	OD	27	44	3	2	8	0	2	22	0
9	RC	9	26	0	0	0	0	2	22	0
	OD	3	2	0	1	0	0	0	0	0
10	RC	0	0	0	0	2	0	0	0	0
	OD	13	17	4	0	1	1	5	3	1
11	RC	27	24	10	4	2	1	5	3	1
	OD	14	7	6	4	3	0	0	0	0
12	RC	0	0	0	0	3	0	0	0	0
	OD	2	7	13	1	3	0	1	1	1
13	RC	27	18	35	4	4	0	3	1	1
	OD	25	11	22	3	4	0	2	0	0

RC*: Reference Case; OD#: Optimized Distribution

Based on the results obtained above, it can be concluded that the distribution model in Step 2 is reliable and effective. The proposed model can provide better distribution options in terms of both noise impact and fuel consumption.

5.2. Evaluation of the entire framework

In this section, the performance of the framework in its entirety is evaluated. However, in Step 1 of the framework, the set of optimized routes for each given SID can be obtained by using either 2D optimization or 3D optimization. For the 2D optimization, only ground tracks are optimized while vertical profiles comply with standard departure procedures, such as Noise Abatement Departure Procedures 1 and 2 (NADP1, NADP2) (ICAO, 2006). For the 3D optimization, both ground tracks and vertical profiles are optimized simultaneously. Therefore, before generating the optimized solutions, a comparison of these two approaches is first carried out in the next subsection. This comparison also aims to provide a better understanding of the final optimized solutions for the complete problem, which will be considered in Section 5.2.2.

5.2.1. A comparison of optimized routes based on the different settings of vertical profiles

In order to evaluate the influence of the vertical profiles, including NADP1, NADP2, and optimized vertical profiles, on the noise impact and fuel consumption, three distinct optimization problems corresponding to three different vertical profile scenarios are performed for an example route. For this comparison, route 3 is used. The evaluation is also a first study that compares the two different settings of vertical profiles in the field of the aircraft route design problem. To determine optimized solutions, the number of aircraft, as indicated in Table 3 for the terminal point ANDIK with an additional 30% of traffic (which accounts for a potential increase in the number of movements due to the application of the distribution algorithm), is applied. For further details on the motivation to add 30% extra traffic, interested readers are encouraged to read Ho-Huu et al. (2019b). For each optimization problem, aircraft of all types follow a shared ground track, but each with its own distinct vertical profile, which is either a standard procedure or an optimized vertical profile. A SID is assumed to start at the end of the runway at an altitude of 35 ft AGL and at a take-off safety speed V_2+10 kts, and to terminate at an altitude of 6,000 ft and an equivalent airspeed of 250 kts. To solve the three optimization problems, the MOEA/D algorithm with a population size of 50 and a maximum of 1,000 generations, as used in Ho-Huu et al. (2017), is applied. To generate optimized routes for each SID in Step 1 of the framework, the same approach is also applied to all the 13 SIDs.

The optimized solutions are shown in Fig. 10. It can be seen in Fig. 10 that, as expected, the optimized vertical profile is the best approach and significantly outperforms NADP1 and NADP2, while NADP2 generally performs better than NADP1. A closer look at Fig. 10 shows that there are still two NADP1-based solutions that dominate some of the NADP2-based solutions. The reason for this is that, due to the focus on climbing in the initial phase of the departure, the airspeed in a NADP1 is lower than for a NADP2. The lower airspeed allows aircraft to make tighter turns over less populated regions while still satisfying the bank angle constraints, as defined by Eq. (5).

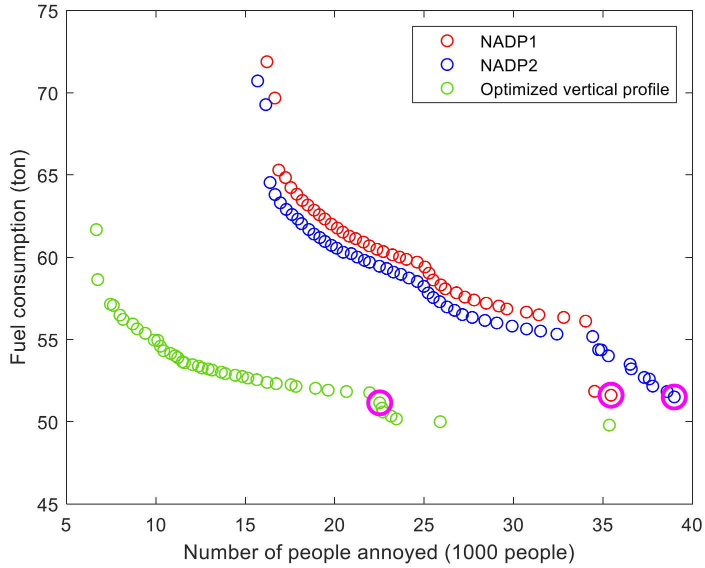

Fig. 10. Comparison of the optimized solutions obtained by NADP1, NADP2 and optimized vertical profiles.

Fig. 11 illustrates the optimized ground tracks obtained for three different optimization problems. It can be observed in Fig. 11 that all ground tracks attempt to avoid populated areas as far as possible. While the differences between the ground tracks obtained by using NADP1 and NADP2 are small, they are quite significant between those obtained by 3D optimization and 2D optimization. For a better understanding of the combination of ground tracks and vertical profiles, some representative solutions of each case, as highlighted in Fig. 11 in yellow, are selected. The vertical profiles derived from a B738 for each approach are depicted in Fig. 12. It is seen in Fig. 12 that there is a significant difference in the airspeed profile between the approaches.

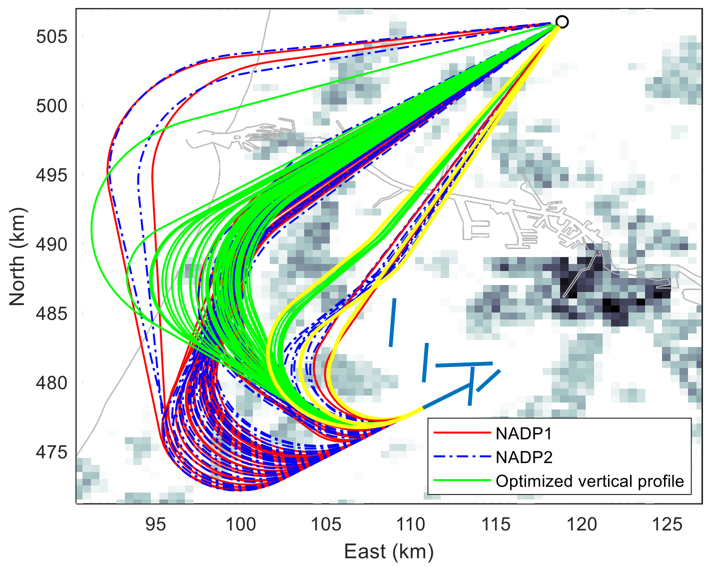

Fig. 11. Comparison of optimized ground tracks obtained by NADP1, NADP2 and optimized vertical profiles.

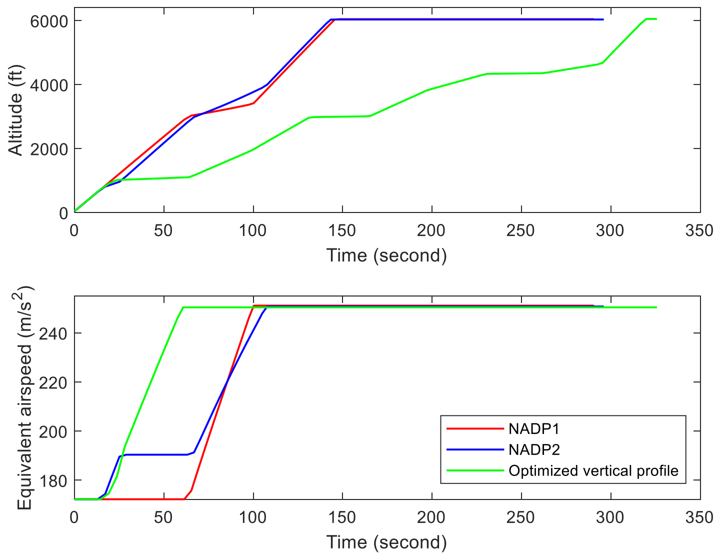

Fig. 12. Comparison of vertical profiles obtained by the representative solutions.

From noise and fuel perspectives, the optimized routes obtained by the 3D optimization approach are the best candidates and should be used in the set of alternative route options for the distribution problem in the second step. From a practical point of view, however, the implementation of the optimized vertical profiles may prove significantly more difficult. In contrast, NADP1 and NADP2 are the current standard procedures that are widely used. Also, compared with NADP1, NADP2 is generally a better option; however, the difference is small. The differences between their vertical profiles, however, may prove useful in dealing with separation conflicts between aircraft. Therefore, to obtain a better understanding from both a theoretical and a practical perspective, two different scenarios in input data are defined for the optimization problem in the second step. In the first scenario, only the routes obtained by NADP1 and NADP2 are applied, while in the second scenario the routes obtained by all the three types of vertical profiles are used. An overview of ground tracks obtained for all the SIDs originating from RW24 and RW18L in both 2D and 3D optimization scenarios is given in Fig. 13.

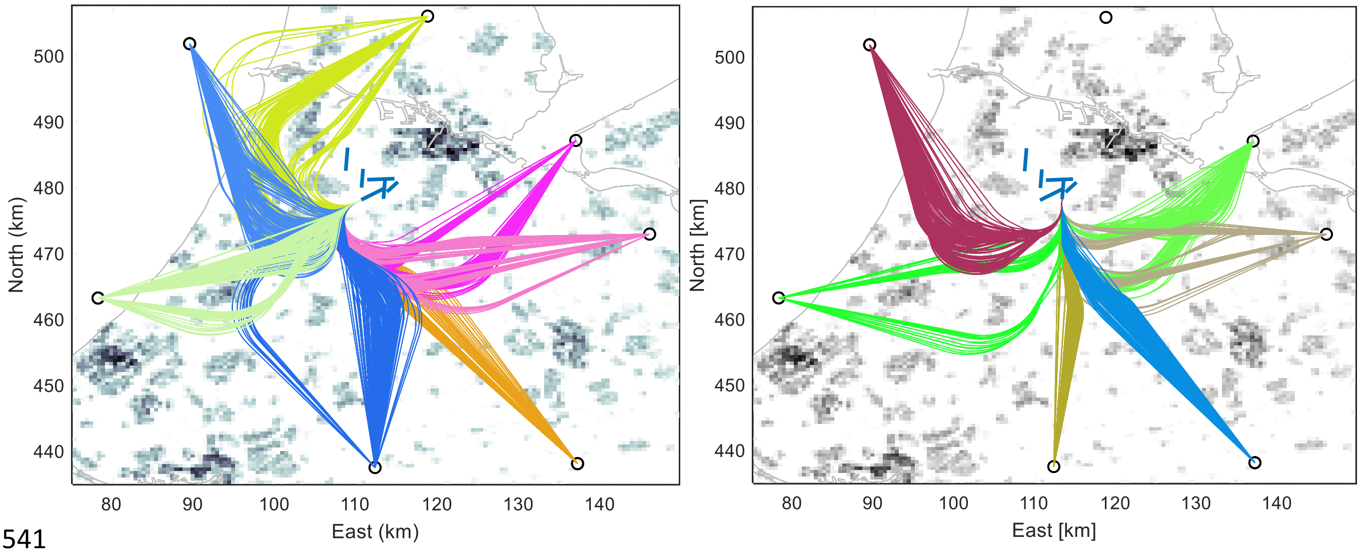

a) RW24 b) RW18L

Fig. 13. Illustration of optimized routes for each SID obtained after Step 1.

5.2.2. Optimized solutions derived from the entire problem

As mentioned earlier, two different sets of input data are considered for the distribution problems in the second step. Therefore, two distinct optimization problems need to be solved in this section. These problems are again referred to as 2D and 3D optimization scenarios, respectively. To solve these problems, the NSGA-II algorithm with a population size of 70 and a maximum number of generations of 1500, as used in Ho-Huu et al. (2019a), is applied.

A closer look at the results obtained for both scenarios reveals that all the solutions obtained by the 3D optimization scenario have a unique route for each SID, while for the solutions obtained by the 2D optimization scenario, some SIDs require two routes to avoid potential conflicts. In addition, there is no delay at the runways for all solutions obtained by both approaches. Fig. 14 shows the Pareto-optimized solutions obtained for the 2D and 3D optimization problems and compares them with the reference case solution, presented previously in Section 5.1. As expected, the 3D optimization approach provides the best solutions (denoted as 3D solutions), that significantly outperform the solutions obtained by the 2D optimization approach (denoted as 2D solutions), as well as those obtained for the reference case, in terms of both the NPA and fuel consumption.

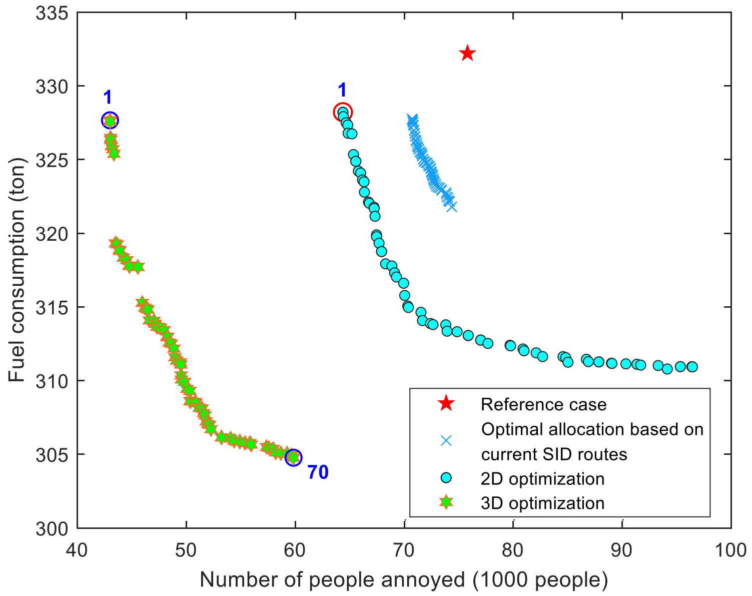

Fig. 14. Comparison of the optimized solutions obtained by the reference case, 2D and 3D optimization.

To further analyze the optimized results, three representative solutions, including solution 1 of the 2D optimization scenario and solutions 1 and 70 of the 3D optimization scenario, as highlighted in Fig. 14, are selected. Table 5 provides a comparison of specific criteria extracted for these solutions. From Table 5, it can be seen that all the compared metrics obtained by solution 1 (2D optimization) and solution 70 are better than those found for the reference case. Specifically, solution 1 offers, respectively, 15.08%, 1.20%, 0.96%, and 0.75% reduction in the NPA, fuel consumption, flight distance and flight time, while the corresponding reductions obtained for solution 70 are, respectively, 21.06%, 8.26%, 8.22% and 8.98%. In a comparison of solution 1 (3D optimization) with the reference case, solution 1 results in a significant decrease in the NPA of about 43.29%, while still saving 1.3% on fuel. Although there is an increase in the flight distance and elapsed time as a result of longer routes to avoid populated regions, the use of optimized vertical profiles results in a fuel burn that is still less than that of the reference case. Note that the purpose of selecting these representative solutions is to merely give insight into the solution behavior; it does not necessarily imply that the selected solutions should be recommended to authorities or policymakers. Essentially, the trade-off between criteria and the subsequent selection of the most desirable solution from the Pareto front is left to the authorities or policymakers.

Table 5. Comparison of the criteria of the representative solutions and the reference case.

Criteria	Solution 1 (2D optimization)	Solution 1 (3D optimization)	Solution 70 (3D optimization)	Reference case
Number of people annoyed	64,367	42,985	59,834	75,800
Fuel consumption (ton)	328.21	327.66	304.77	332.20
Flight distance (km)	25,240.57	27,357.49	23,388.53	25,484.13
Flight time (h)	56.71	59.80	52.01	57.14

The explanations provided for the comparisons in Table 5 are confirmed by the results shown in Figs. 15- 17. where the optimized routes, the L_{den} noise contours, and the NPA obtained by the three solutions are illustrated. A closer look at the optimized routes shows that although the optimized routes selected by these solutions are different, all of them seek to avoid high-density residential areas and tend to be close to each other. This results in narrower L_{den} contours and hence a reduced number of people affected by noise. Another observation is that the routes selected in solutions 1 (both 2D and 3D optimization) are longer than those selected by solution 70. This is according to expectations, as both solutions for 1 are noise-preferred solutions, and hence their routes tend to be longer to avoid populated regions. In contrast, solution 70 is a fuel-preferred solution and therefore prefers to choose shorter routes to reduce the fuel burn. Note that the red routes in Fig. 15 (solution 1 of 2D problem) are two alternative routes that are only used by some conflicting flights, whilst the remainder of the scheduled flights make use of one of the blue routes for each SID.

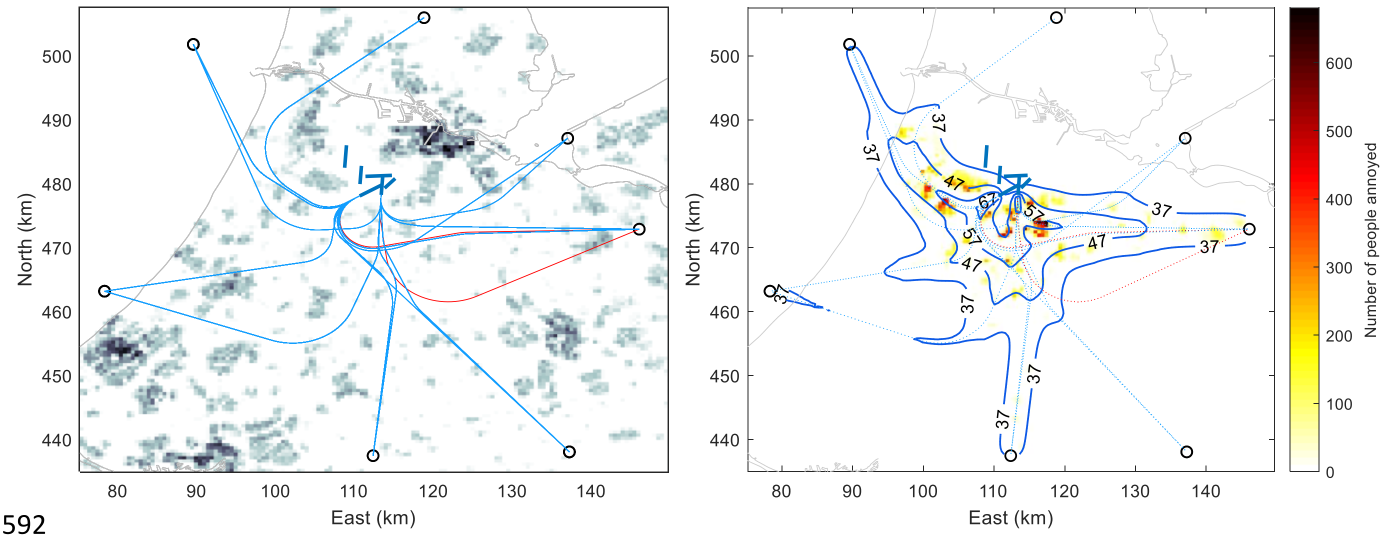

a) Optimized routes b) L_{den} noise contours and the NPA

Fig. 15. Illustration of the optimized routes, the L_{den} noise contours, and the NPA (solution 1 – 2D optimization).

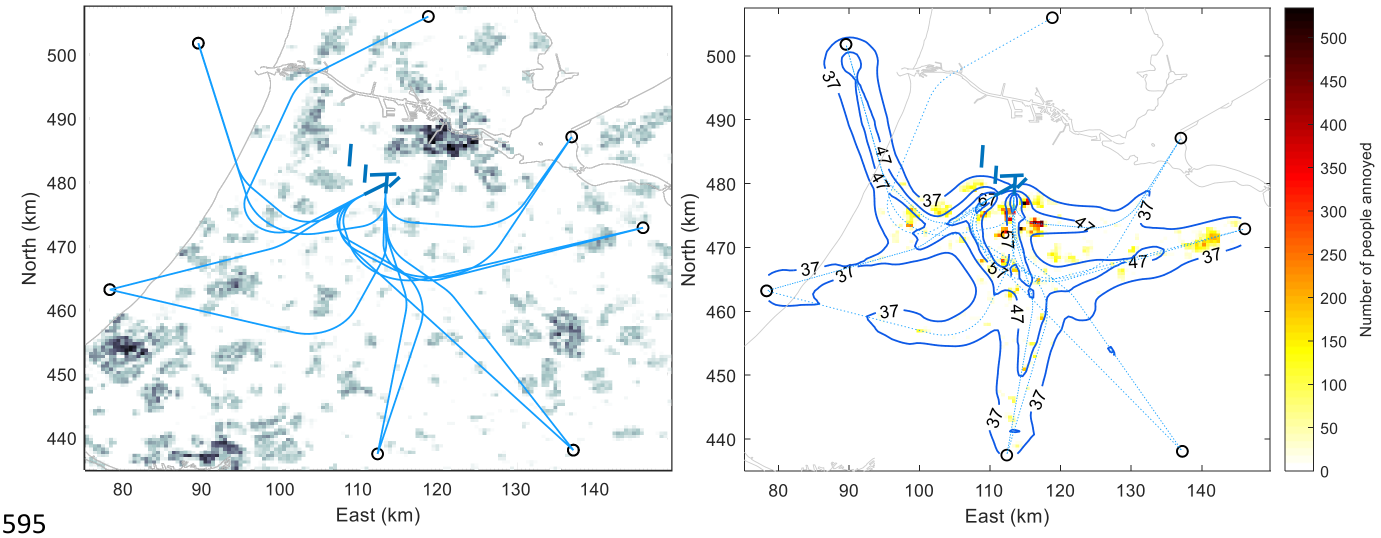

a) Optimized routes b) L_{den} noise contours and the NPA

Fig. 16. Illustration of the optimized routes, the L_{den} noise contours, and the NPA (solution 1 – 3D optimization).

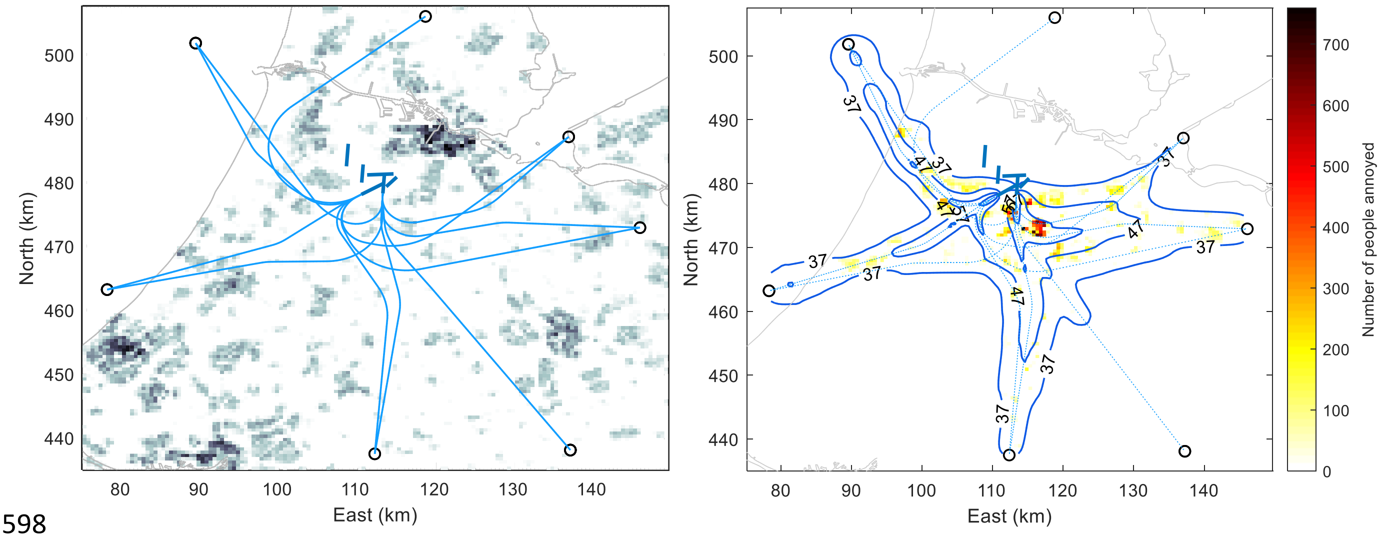

a) Optimized routes b) L_{den} noise contours and the NPA

Fig. 17. Illustration of the optimized routes, the L_{den} noise contours, and the NPA (solution 70 – 3D optimization).

Table 6 provides the detailed distribution of flights among the optimized routes obtained in the selected solutions. It should be noted that as the selection of routes and the distribution of flights among these routes are optimized simultaneously, each solution will have its own optimized combination of selected routes and flight distribution. Therefore, it is difficult to make a direct comparison regarding the aircraft distribution between them, especially the comparison between 2D and 3D solutions. As a result, Table 6 merely aims to give insight into the optimized solution behavior, rather than serving as a basis for comparison.

Table 6. Distribution of flights to the optimized routes obtained by the 2D and 3D representative solutions.

Route number	Solution	Day			Evening			Night		
		F100	B738	B773	F100	B738	B773	F100	B738	B773
1	1 (2D)	6	0	0	0	0	0	0	0	0
	1 (3D)	4	11	0	0	4	1	0	2	0
	70 (3D)	12	11	2	1	4	3	5	2	0
2	1 (2D)	3	1	0	0	0	0	7	2	0
	1 (3D)	0	0	3	0	0	4	6	0	0
	70 (3D)	0	0	1	0	0	2	2	0	0
3	1 (2D)	23	13	3	6	6	5	0	0	0
	1 (3D)	28	3	0	6	2	0	1	0	0
	70 (3D)	20	3	0	5	2	0	0	0	0
4	1 (2D)	5	38	9	1	5	8	0	19	3
	1 (3D)	30	37	15	4	4	10	8	19	2
	70 (3D)	4	11	4	0	1	6	0	1	0
5	1 (2D)	52	31	19	8	5	4	8	0	0
	1 (3D)	27	32	13	5	6	2	0	0	1
	70 (3D)	53	58	24	9	9	6	8	18	3
6	1 (2D)	2	7	2	2	1	0	0	1	0
	1 (3D)	2	9	1	2	1	0	0	1	0
	70 (3D)	4	9	2	2	1	0	1	1	0
7	1 (2D)	2	2	0	0	0	0	1	0	0
	1 (3D)	2	0	1	0	0	0	1	0	0
	70 (3D)	0	0	0	0	0	0	0	0	0
8	1 (2D)	25	16	3	2	5	0	2	0	0
	1 (3D)	28	44	3	2	7	0	2	22	0
	70 (3D)	28	44	3	2	7	0	2	22	0
9	1 (2D)	5	30	0	1	3	0	0	22	0
	1 (3D)	2	2	0	1	1	0	0	0	0
	70 (3D)	2	2	0	1	1	0	0	0	0
10	1 (2D)	12	19	4	0	2	1	5	3	1
	1 (3D)	9	17	1	0	2	1	5	3	1
	70 (3D)	3	9	0	0	0	0	1	1	0
11	1 (2D)	15	5	6	4	2	0	0	0	0
	1 (3D)	18	7	9	4	2	0	0	0	0
	70 (3D)	24	15	10	4	4	1	4	2	1
12	1 (2D)	0	7	0	0	2	0	1	1	0
	1 (3D)	0	2	0	0	1	0	0	0	0
	70 (3D)	0	3	0	0	0	0	0	0	0
13	1 (2D)	27	11	35	4	5	0	2	0	1
	1 (3D)	27	16	35	4	6	0	3	1	1
	70 (3D)	27	15	35	4	7	0	3	1	1

In order to make the comparison regarding the vertical profiles more transparent, the representative vertical profiles of a Fokker 100 obtained for solutions 1 (both 2D and 3D optimization) are depicted in Fig. 18. As expected, despite not having the best performance in terms of either noise or fuel burn, NADP1 is still selected in both the 2D and 3D solutions, merely because it helps avoid conflicts. However, due to its poor performance, it is rarely used. More specifically, for both the 2D and 3D solutions, only 1 route selects NADP1 as the optimized option, while the remainder chooses either NADP2 or the optimized vertical profiles. The selection of NADP1 has shown that the separation requirement is an important and challenging issue that will be very difficult to solve if only one type of vertical profiles is available for all aircraft movements, especially for operations at peak hours. This issue again can be seen in the 3D solution. In this solution, even though the optimized vertical profile offers the best performance in both criteria, only 7 routes use it as the optimized option, while there are still 4 routes using NADP2 and 1 route using NADP1. Thanks to the combination of all three different vertical profiles, the 3D optimized solutions are the only ones that offer conflict-free solutions by using only one route for each SID for the entire flight schedule.

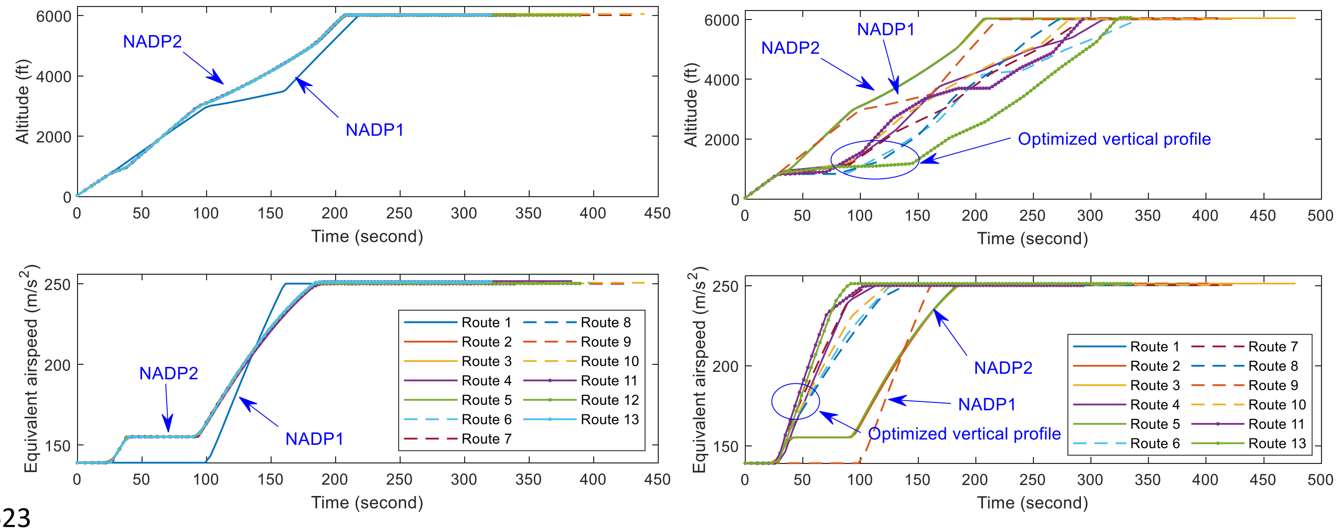

a) Solution 1 (2D optimization) b) Solution 1 (3D optimization)

Fig. 18. Comparison of the vertical profiles of Fokker 100 obtained by 2D and 3D optimization.

6. Conclusions

In this paper, we have presented a multilevel optimization framework for the design of optimal departure routes and the distribution of aircraft movements among these routes, while taking the sequence and separation constraints of aircraft into account. The proposed framework consists of two successive steps: 1) the design of optimal routes for each SID, and 2) the selection and distribution of flights among these routes. In order to deal with the sequence and separation requirements for aircraft, a runway assignment model, a conflict detection algorithm, and a rerouting technique have also been developed.

The performance and applicability of the proposed framework have been demonstrated through a case study at Amsterdam Airport Schiphol (AMS) in The Netherlands. In this case study, the departure operations for an entire day, featuring 599 flights and 13 distinct routes, have been considered. First, to validate the integration of the runway assignment model and the conflict detection algorithm into the allocation model in Step 2, a pure allocation problem based on the current SIDs has been executed. The obtained results reveal that the distribution model is reliable and able to provide better options that help significantly reduce the noise impact and fuel consumption compared with the reference case. Subsequently, optimized solutions have been generated using the fully integrated framework. In order to provide a better view from both theoretical and practical perspectives, two different settings of input data for the distribution model in Step 2 have also been assessed. The numerical results have revealed that both problems can provide solutions that are much better in terms of both noise and fuel, relative to the reference case. Also, the 3D optimization approach significantly outperforms the 2D optimization approach.

In view of the attained favorable results, the framework appears to be suitable for expansion to other applications such as the design of arrival routes and the allocation of flights among these routes, and the problem that considers both departure and arrival operations concurrently. Moreover, instead of using the rerouting technique in the developed framework, at some occasions, Air Traffic Controllers could implement small delays on the ground or slow down or speed up one of the conflicting flights without changing the given SIDs to avoid conflict in the air. These considerations can also be integrated into the developed framework in future research. In addition, since the results obtained by the framework are Pareto solutions, it is a challenge for potential users to choose a suitable solution from a given Pareto front. Therefore, the development of selection methods and more in-depth analyses of the optimized results are necessary in future work.

References

Asensio, C., Gasco, L., de Arcas, G., 2017. A Review of Non-Acoustic Measures to Handle Community Response to Noise around Airports. Curr. Pollut. Reports 230–244. https://doi.org/10.1007/s40726-017-0060-x

Boeing, 2016. Current Market Outlook 2016–2035.

Braakenburg, M.L., Hartjes, S., Visser, H.G., 2011. Development of a Multi-Event Trajectory Optimization Tool for Noise-Optimized Approach Route Design. AIAA J. 1–13. https://doi.org/10.2514/6.2011-6929

Casalino, D., Diozzi, F., Sannino, R., Paonessa, A., 2008. Aircraft noise reduction technologies: A bibliographic review. Aerosp. Sci. Technol. 12, 1–17. https://doi.org/10.1016/j.ast.2007.10.004

Centraal Bureau voor de Statestiek. Dataset bevolkingsdichtheid. https://www.cbs.nl/nl-nl/ dossier/nederland-regionaal/geografische-data. Online, accessed 2016-10-20.

Chatelain, P., Van Vyve, M., 2018. Modeling fair air traffic assignment in the vicinity of airports. Transp. Res. Part D Transp. Environ. 65, 213–228. https://doi.org/10.1016/j.trd.2018.08.016

D’Ariano, A., Pacciarelli, D., Pistelli, M., Pranzo, M., 2015. Real-time scheduling of aircraft arrivals and departures in a terminal maneuvering area. Networks, 65(3) 212–227. https://doi.org/10.1002/net.21599

Deb, K., Pratap, A., Agarwal, S., Meyarivan, T., 2002. A fast and elitist multiobjective genetic algorithm: NSGA-II. IEEE Trans. Evol. Comput. 6, 182–197. https://doi.org/10.1109/4235.996017

J.G. Delsen., 2016. Flexible Arrival & Departure Runway Allocation Using Mixed-Integer Linear Programming:

A Schiphol Airport Case Study, MSc. thesis, Delft University of Technology.
Dons, J., 2012. Optimization of Departure and Arrival Routing for Amsterdam Airport Schiphol- A Noise Abatement Study. MSc. thesis, Delft University of Technology.
ECAC, 2016. ECAC.CEAC Doc 29 4th Edition Report on Standard Method of Computing Noise Contours around Civil Airports Volume 1: Applications Guide 1.
EUROCONTROL, 2014b. User Manual for the Base of Aircraft Data (BADA) Rev. 3.12, EEC Technical/Scientific Report No. 12/11/22-58.
EUROCONTROL, 2018. RECAT-EU - European Wake Turbulence Categorisation and Separation Minima on Approach and Departure. Brussels. http://www.recat-project.eu/sites/default/files/20180214_recat-eu_presentation_brochure_v1.2.pdf
European Environment Agency (EEA), 2010. Good practice guide on noise exposure and potential health effects, n.d. , in: EEA Technical Report.
Filippone, A., 2014. Aircraft noise prediction. Prog. Aerosp. Sci. 68, 27–63. https://doi.org/10.1016/j.paerosci.2014.02.001
Frair, L., 1984. Airport noise modelling and aircraft scheduling so as to minimize community annoyance. Appl. Math. Model. 8, 271–281. https://doi.org/10.1016/0307-904X(84)90162-8
Ganić, E., Babić, O., Čangalović, M., Stanojević, M., 2018. Air traffic assignment to reduce population noise exposure using activity-based approach. Transp. Res. Part D Transp. Environ. 63, 58–71. https://doi.org/10.1016/j.trd.2018.04.012
Gardi, A., Sabatini, R., Ramasamy, S., 2015. Multi-objective optimisation of aircraft flight trajectories in the ATM and avionics context. Prog. Aerosp. Sci. 83, 1–36. https://doi.org/10.1016/j.paerosci.2015.11.006
Hartjes, S., Dons, J., Visser, H.G., 2014. Optimization of Area Navigation Arrival Routes for Cumulative Noise Exposure. J. Aircr. 51, 1432–1438. https://doi.org/10.2514/1.C032302
Hartjes, S., Visser, H., 2016. Efficient trajectory parameterization for environmental optimization of departure flight paths using a genetic algorithm. Proc. Inst. Mech. Eng. Part G J. Aerosp. Eng. 0, 1–9. https://doi.org/10.1177/0954410016648980
Hartjes, S., Visser, H.G., Hebly, S.J., 2010. Optimisation of RNAV noise and emission abatement standard instrument departures. Aeronaut. J. 114, 757–767. https://doi.org/10.1017/CBO9781107415324.004
Ho-Huu, V., Ganić, E., Hartjes, S., Babić, O., Curran, R., 2019a. Air traff assignment based on daily population mobility to reduce aircraft noise effcts and fuel consumption. Transp. Res. Part D Transp. Environ. 72, 127–147. https://doi.org/10.1016/j.trd.2019.04.007
Ho-Huu, V., Hartjes, S., Visser, H., Curran, R., 2017. An Efficient Application of the MOEA/D Algorithm for Designing Noise Abatement Departure Trajectories. Aerospace 4, 54. https://doi.org/10.3390/aerospace4040054
Ho-Huu, V., Hartjes, S., Visser, H.G., Curran, R., 2019b. An optimization framework for the design and allocation of aircraft to multiple departure routes. Transp. Res. Part D Transp. Environ. 76, 273-288. https://doi.org/10.1016/j.trd.2019.10.003
Ho-Huu, V., Hartjes, S., Visser, H.G., Curran, R., 2018. Integrated design and allocation of optimal aircraft departure routes. Transp. Res. Part D Transp. Environ. 63, 689–705. https://doi.org/10.1016/j.trd.2018.07.006
Hogenhuis, R.H., Hebly, S.J., Visser, H.G., 2011. Optimization of area navigation noise abatement approach trajectories. Proc. Inst. Mech. Eng. Part G-Journal Aerosp. Eng. 225, 513–521. https://doi.org/10.1177/09544100JAERO840
International Civil Aviation Organization (ICAO), 2006a. Procedures for air navigation services – Aircraft operations. Vol. I, Flight Procedures.
International Civil Aviation Organization (ICAO), 2016b. Doc 4444 – Procedures for air navigation services – Air traffic management. Sixteenth Edition. Montreal, QC, Canada.
Isaacson, D.R., Erzberger, H., 1997. Design of a conflict detection algorithm for the Center/TRACON automation system, in: 16th DASC. AIAA/IEEE Digital Avionics Systems Conference. Reflections to the Future. Proceedings. pp. 9.3–1. https://doi.org/10.1109/DASC.1997.637306
Janssen, S.A., Centen, M.R., Vos, H., Van Kamp, I., 2014. The effect of the number of aircraft noise events on sleep quality. Appl. Acoust. 84, 9–16. https://doi.org/10.1016/j.apacoust.2014.04.002
Kuiper, B.R., Visser, H.G., Heblij, S., 2012. Efficient use of an allotted airport annual noise budget through minimax optimization of runway allocations. Proc. Inst. Mech. Eng. Part G J. Aerosp. Eng. 227, 1021–1035. https://doi.org/10.1177/0954410012447767
Morrell, S., Taylor, R., Lyle, D., 1997. A review of health effects of aircraft noise. Aust. N. Z. J. Public Health 21, 221–236. https://doi.org/10.1111/j.1467-842X.1997.tb01690.x
Prats, X., Puig, V., Quevedo, J., 2011. Equitable Aircraft Noise-Abatement Departure Procedures. J. Guid. Control. Dyn. 34, 192–203. https://doi.org/10.2514/1.49530
Prats, X., Puig, V., Quevedo, J., Nejjari, F., 2010a. Lexicographic optimisation for optimal departure aircraft

trajectories. Aerosp. Sci. Technol. 14, 26–37. https://doi.org/10.1016/j.ast.2009.11.003

Prats, X., Puig, V., Quevedo, J., Nejjari, F., 2010b. Multi-objective optimisation for aircraft departure trajectories minimising noise annoyance. Transp. Res. Part C Emerg. Technol. 18, 975–989. https://doi.org/10.1016/j.trc.2010.03.001

Rodríguez-Díaz, A., Adenso-Díaz, B., González-Torre, P.L., 2017. A review of the impact of noise restrictions at airports. Transp. Res. Part D Transp. Environ. 50, 144–153. https://doi.org/10.1016/j.trd.2016.10.025

Samà, M., D'Ariano, A., D'Ariano, P., Pacciarelli, D., 2017a. Scheduling models for optimal aircraft traffic control at busy airports: tardiness, priorities, equity and violations considerations. Omega 67(1), 81–98. https://doi.org/10.1016/j.omega.2016.04.003

Samà, M., D'Ariano, A., Corman, F., Pacciarelli, D., 2017b. Metaheuristics for efficient aircraft scheduling and re-routing at busy terminal control areas. Transp. Res. Part C 80 (1), 485–511. https://doi.org/10.1016/j.trc.2016.08.012

Samà, M., D'Ariano, A., Corman, F., Pacciarelli, D., 2018. Coordination of scheduling decisions in the management of airport airspace and taxiway operations, Transp. Res. Proce. 23, 246-262. https://doi.org/10.1016/j.trpro.2017.05.015

Samà, M., D'Ariano, A., Palagachev, K., Gerdts, M., 2019. Integration methods for aircraft scheduling and trajectory optimization at a busy terminal manoeuvring area. OR Spec. 41, 641–681. https://doi.org/10.1007/s00291-019-00560-1

Song, Z., Visser, H.G., Mingshan, H., Wei, C., 2014. Optimized Multi-Event Simultaneous Departure Routes for Major Hub Airport. Int. J. Model. Optim. 4, 482–488. https://doi.org/10.7763/IJMO.2014.V4.421

Storn, R., Price, K., 1997. Differential Evolution – A Simple and Efficient Heuristic for global Optimization over Continuous Spaces. J. Glob. Optim. 11, 341–359. https://doi.org/10.1023/A:1008202821328

Torres, R., Chaptal, J., Bès, C., Hiriart-Urruty, J.-B., 2011. Optimal , Environmentally Friendly Departure Procedures for Civil Aircraft. J. Aircr. 48, 11–23. https://doi.org/10.2514/1.C031012

Visser, H.G., 2008. Environmentally optimized resolutions of in-trail separation conflicts for arrival flights. J. Aircr. 45, 1198–1205. https://doi.org/10.2514/1.34090

Visser, H.G., Wijnen, R.A.A., 2003. Optimisation of noise abatement arrival trajectories. Aeronaut. J. 107, 607–615. https://doi.org/10.1017/S0001924000013828

Visser, H.G., Wijnen, R.A.A., 2001. Optimization of Noise Abatement Departure Trajectories. J. Aircr. 38, 620–627. https://doi.org/10.2514/2.2838

Yu, H., Van Kampen, E.-J., Mulder, J.A., 2016. An Optimization Paradigm for Arrival Trajectories usingTrajectory Segmentation and State Parameterization. AIAA Guid. Navig. Control Conf. 1–17. https://doi.org/10.2514/6.2016-1872

Zachary, D.S., Gervais, J., Leopold, U., 2010. Multi-impact optimization to reduce aviation noise and emissions. Transp. Res. Part D Transp. Environ. 15, 82–93. https://doi.org/10.1016/j.trd.2009.09.005

Zachary, D.S., Gervais, J., Leopold, U., Schutz, G., Huck, V.S.T., Braun, C., 2011. Strategic Planning of Aircraft Movements with a Three-Cost Objective. J. Aircr. 48, 256–264. https://doi.org/10.2514/1.C031090

Zaporozhets, O.I., Tokarev, V.I., 1998. Predicted flight procedures for minimum noise impact. Appl. Acoust. 55, 129–143. http://dx.doi.org/10.1016/S0003-682X(97)00108-4

Zhang, M., Filippone, A., Bojdo, N., 2018. Multi-objective optimisation of aircraft departure trajectories. Aerosp. Sci. Technol. 79, 37–47. https://doi.org/10.1016/j.ast.2018.05.032

Zhang, Q., Li, H., 2007. MOEA/D: A Multiobjective Evolutionary Algorithm Based on Decomposition. IEEE Trans. Evol. Comput. 11, 712–731. https://doi.org/10.1109/TEVC.2007.892759